CONF-9610170--4
SAND96-2571C

Shock-Wave Properties of Soda-Lime Glass

Dennis E. Grady
Applied Research Associates, Inc.
4300 San Mateo Blvd., NE, Suite A-220
Albuquerque, NM 87110

Lalit C. Chhabildas
Sandia National Laboratories
Albuquerque NM 871580-0821

Abstract

The shock-wave properties of soda-lime glass have been investigated through the use of planar impact experiments and wave profile measurements using time-resolved velocity interferometry. The experiments provided both single and double shock equation-of-state data to approximately 30 GPa. Both compression wave profile structure and release wave data were used to infer time-dependent strength and equation-of-state properties for soda-lime glass.

Introduction

The reported Hugoniot elastic limit for soda-lime glass is 6.4 - 7.0 GPa [Rosenberg et al., 1985]. However, complex time-dependent failure processes in similar glass at significantly lower shock stresses were reported by Kanel et al. (1992). Further evidence for failure kinetics in soda-lime glass at shock stresses below the HEL provided in subsequent studies [Brar et al., 1991; Rasorenov et al., 1991; Dandekar and Beaulieu et al., 1995; Bourne and Rosenberg, 1996].

Lacking in this research has been a detailed study of shock profile structure in soda-lime glass spanning the stress range encompassing the reported Hugoniot elastic limit and failure kinetics features. The present investigation reports new time-resolved velocity interferometry data providing shock and release profile structures in soda-lime glass. The equation-of-state and dynamic strength behavior of soda-lime glass revealed by these shock data are examined for further enlightenment on the complex deformation characteristics of this material.

This work was supported by the United States Department of Energy under Contract DE-AC04-94AL85000.
Sandia is a multiprogram laboratory operated by Sandia Corporation, a Lockheed Martin Company, for the United States Department of Energy.

DISCLAIMER

Material Characteristics and Experimental Method

The present soda-lime glass is the same material investigated in earlier studies [Anderson et al., 1993; Senf et al., 1994; Holmquist et al., 1995]. The material was provided by Dr. Volker Hohler of the Ernst-Mach Institute, Freiburg, Germany. Measured density of the glass was 2530 kg/m^3. Measured longitudinal and shear ultrasonic velocities were 5.83 km/s and 3.47 km/s, respectively. Bulk modulus, shear modulus and Poisson's ratio calculated from the elastic wave speeds were 45.3 GPa, 30.4 GPa and 0.226, respectively. The oxide composition in percent by mass was SiO_2(37.2), Na_2O(10.6), CaO(9.4), MgO(3.1), Al_2O_3(1.8), K_2O(1.1) and Fe_2O_3(0.2).

Strength properties other than shock wave data which have been measured for this glass [Holmquist et al., 1995] include static unconfined compression tests, compression Hopkinson bar and static biaxial tests to determine tensile strengths.

The experimental configuration is schematically illustrated in Figure 1. Tests were performed on an 89 mm smooth-bore powder gun. Projectile velocity was measured with electrical shorting pins to an accuracy of $\pm 1\%$. Stationary test targets were constructed of discs of the soda-lime glass back by discs of optical quality lithium fluoride bonded to the glass sample. The projectile carried a impactor disc of the same soda-lime glass or, in the experiments achieving the highest shock stresses, discs of copper. In either case the impacting disc was backed by a low impedance material (20 lb/ft^3 foam for glass or pmma for copper) to achieve a following decompression wave. The velocity history induced by the planar impact was, in each case, recorded at the interface between the glass and the lithium-fluoride window.

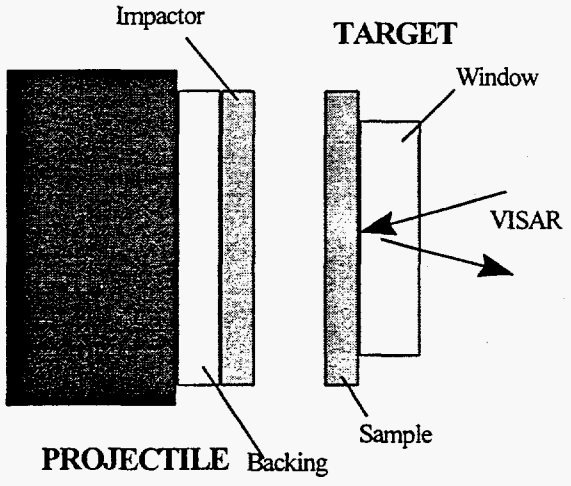

Figure 1: Experimental configuration for wave-profile measurements.

Experimental Profiles and Observations

Compression wave profiles for the eight shock wave experiments on glass are shown together in Figure 2. Profiles for the four higher amplitude experiment exhibit a systematic variation in the compression wave structure with increasing shock amplitude. The elastic precursor waves for these tests are dispersive, manifesting the initial anomalous (softening) elastic modulus characteristic of glasses.

The profiles in this dispersive region overlay, illustrating the very good experimental reproducibility of this material and the VISAR diagnostic.

Tests AT-1 and AT-9 were performed under the same impact conditions (Table 1) as were tests AT-2 and AT-8. Profiles for the latter two test differ strikingly from other test in the present series. Velocity histories for the two tests exhibit chaotic motion and the two profiles do not overlay although they tend to converge toward a similar peak amplitude near the end of the profiles.

Table 1: Test Parameters

Test Num.	Impact Vel. (km/s)	Backing Material	Backing Thickness (mm)	Impactor Material	Impactor Thickness (mm)	Target Thickness (mm)	Window Thickness (mm)
AT-1	0.65	foam	6.27	glass	6.00	5.98	25.5
AT-2	1.33	foam	6.36	glass	6.00	5.98	25.5
AT-3	1.99	foam	6.31	glass	6.01	6.00	25.4
AT-4	2.38	foam	6.35	glass	6.02	6.00	18.9
AT-5	1.94	pmma	12.8	copper	2.35	5.96	25.5
AT-6	2.33	pmma	12.8	copper	2.38	5.98	25.4
AT-8	1.35	foam	6.27	glass	6.01	5.98	25.4
AT-9	0.64	foam	4.93	glass	5.98	5.97	25.4

Hugoniot States

The peak compression states of stress, strain and particle velocity (Hugoniot states) were extracted from the wave profile data. by approximating the measured wave profiles by two shocks; an elastic shock with a velocity of 5.83 km/s and amplitude selected at 0.4 km/s, and a deformational shock wave of velocity determined by the arrival of the wave midpoint. These properties, combined with symmetry of impact, allowed calculation of the Hugoniot states.

The elastic wave selected at a representative amplitude of the precursor wave of 0.4 km/s corresponds to stress level of 6.0 GPa. This stress should not be construed as a Hugoniot elastic limit. The transition from elastic to inelastic behavior, discussed later, is not clearly revealed in the present wave profiles.

A reshock of the glass occurred in the higher impact amplitude tests because of a reflected shock at the lithium fluoride interface. Pressure and particle velocity behind the second shock are established by the peak amplitude of the VISAR profile and the known Hugoniot relation for lithium fluoride. Velocity of the second shock U and the change in specific volume Δv across the shock are given by $U = \Delta p/\rho_o \Delta u$ and $\Delta v = (\Delta u)^2/\Delta p$ where Δp and Δu are the jumps in

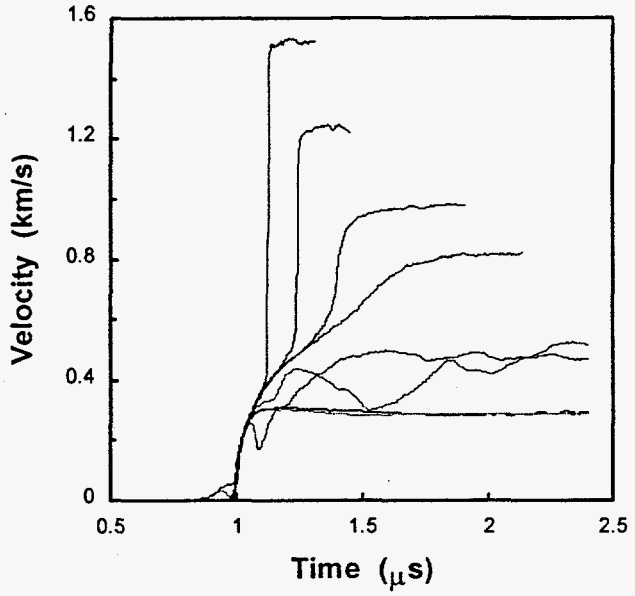

Figure 2: Compression profiles for soda-lime glass.

pressure and particle velocity, respectively. Stress-versus-specific-volume compression states for the first and second shock Hugoniot data are shown in Figure 4.

Crystalline SiO_2 in tetrahedral coordination is known to transform to the more dense octahedral coordination at a pressure of about 15 GPa. First order estimates of the compression curves for the present glass are shown in Figure 4. Zero pressure densities have been estimated from the glass chemistry while compressibility of pure SiO_2 in the quartz (tetrahedral) phase and stishovite (octahedral) phase were used to estimate compression at pressure. Significant transformation of the present glass to the dense phase is not indicated by the present first and second shock data to nearly 30 GPa.

Release Velocities.

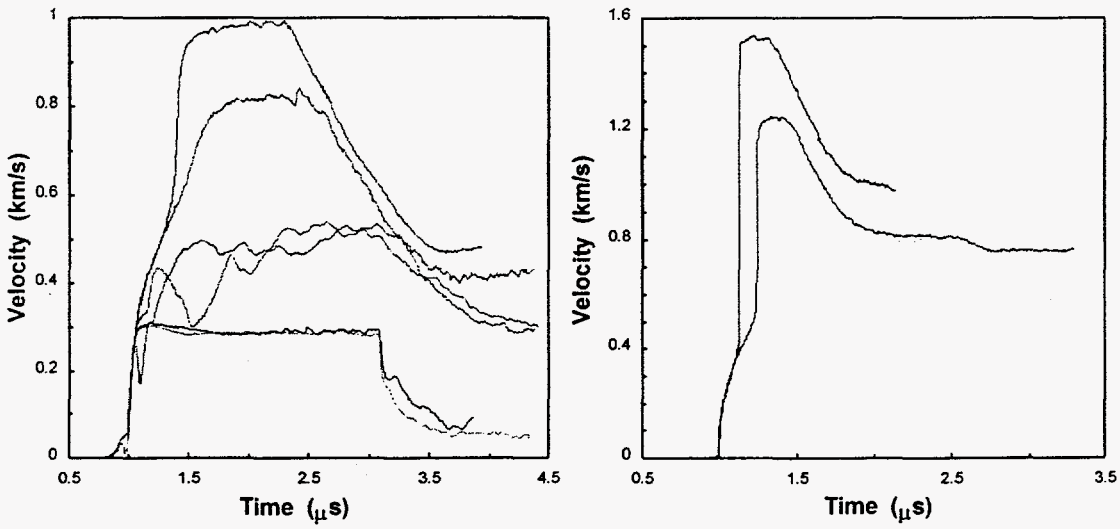

Figure 3: Measured wave profiles for glass (left) and copper (right) impactors.

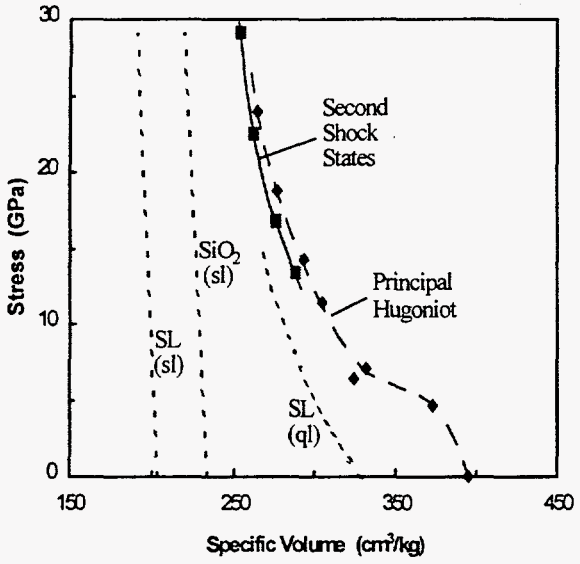

Figure 4: First and second experimental shock states for glass. Reference compression curves are, respectively, pure SiO_2 in stishovite phase - SiO_2(sl); stishovite-like compression corrected for soda-lime chemistry - SL(sl); and quartz-like compression corrected for soda-lime chemistry - SL(ql).

The impacting plate striking the stationary glass and lithium fluoride target assembly is backed by a lower mechanical impedance material (foam or pmma). Consequently, the impact-induced compression wave incident on this interface is reflected as a release wave which decompresses the shock state in the glass sample. The first arrival of this release profile is an acceleration wave which provides a measure of the sonic velocity at the stress amplitude of the Hugoniot state. Sonic velocities established from the release profiles are provided in Table 2. Sonic release velocity data are shown Figure 5. These data are compared with other velocity measures determined from the wave profiles including principal shock velocity, second shock velocity and velocity of the dispersive compression precursor wave.

Discussion

The nature of finite amplitude shock waves measured in this study have revealed a richness and complexity unexpected in common window glass. Although many of the observed features are understood within the framework of standard shock wave analysis, other features are unique to this glass and elude a simple explanation.

Hugoniot Elastic Limit

Precursor waves in the shock compression of solids are common and usually characterize a transition from elastic to inelastic behavior as a bulk or shear strength limit of the material is achieved. This strength limit, usually called the Hugoniot elastic limit, is typically estimated from the amplitude of this precursor wave. Precursor waves can originate in solids exhibiting strictly elastic behavior and the elastic characteristics which lead to precursor waves are,

in fact, common to many glassy materials. If the material initially displays elastic softening under compression then a dispersing precursor wave like that exhibited by the data in Figure 2 is expected. Thus, *the existence of a precursor wave in the present glass does not in of itself indicate a dynamic strength limit.* The wave profile data must be looked at in more detail for evidence of transition to inelastic behavior.

Consider the two lowest impact amplitude experiments AT-1 and AT-9. Compressive stress amplitudes of approximately 4.6 GPa were achieved in these tests - below reported Hugoniot elastic limit values for soda-lime glass (Rosenberg et al., 1985). The compression wave is dispersive and the release is sharp, and with a velocity (see Figure 5), consistent with an elastic rarefaction shock. This would indicate strict elastic behavior at this shock stress amplitude. There are, however, several unsettling features in the wave profiles for AT-1 and AT-9. In both tests the profile reaches a peak particle velocity and then relaxes over about 0.5 μs to a level about 25 m/s less than the peak - a behavior also noted by Bourne and Rosenberg, (1996). It is difficult to think of an experimental artifact that would produce this behavior in both tests. Stress relaxation associated with a small level of permanent densification or inelastic shear must be considered.

Table 2: First and Second Shock Hugoniot States

Test Num.	Stress (GPa)	Spec. Volume (cm^3/kg)	Particle Vel. (km/s)	Shock Vel. (km/s)	Stress (GPa)	Spec. Volume (cm^3/kg)	Shock Vel. (km/s)	Release[1] Vel. (km/s)
	First Shock Hugoniot State				Second Hugoniot State			
AT-1	4.66	372.4	0.324	*	*	*	*	5.74(±1%)
AT-2	7.0	332.0	0.664	*	*	*	*	5.25(±3%)
AT-3	11.46	304.4	0.995	3.68	13.45	288.1	4.37	7.74(±5%)
AT-4	14.25	293.4	1.190	4.17	16.76	275.8	4.73	8.90(±2%)
AT-5	18.76	276.5	1.485	4.68	22.58	262.0	6.43	11.51(±6%)
AT-6	23.91	264.2	1.768	5.20	29.17	253.4	8.74	13.28(±7%)
AT-8	6.4	324.0	0.674	*	*	*	*	5.58(±5%)
AT-9	4.62	373.1	0.321	*	*	*	*	5.75(±1%)

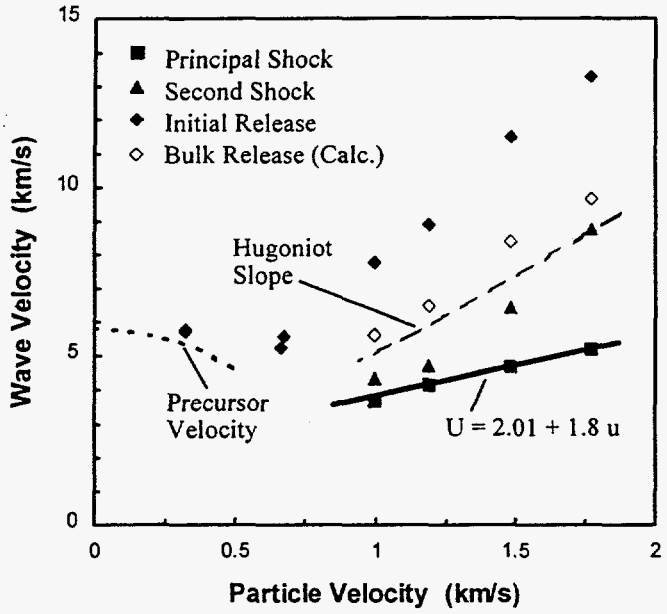

Figure 5: Wave-velocity data for soda-lime glass.

The second disturbing feature is that the plateau particle velocity accounting for the very small impedance correction at the lithium fluoride interface is about 30 m/s or about 10% too low to be consistent with a symmetric impact. Experimental difficulties cannot be ruled out but seem unlikely. Therefore, some inelastic time-dependent process appears to be delaying arrival of the impact interface velocity (one-half of the impact velocity) at the recording interface before the process is quenched by arrival of the release wave. Since the impact interface velocity is not achieved by the arrival of the release wave (~ 3 μs) this feature would have to be propagating at a velocity less than 2 km/s. Such a delayed wave would imply an additional compressive strain of not less than 1.5%. Also the similarities to the compression anomaly reported by Bourne and Rosenberg (1996) attributed by them to irreversible densification should be noted.

Wave profiles for tests AT-2 and AT-8, conducted at approximately twice the impact velocity of the lowest amplitude tests, were found to be starkly different in character. Maximum compressive stresses achieved in tests AT-2 and AT-8 were about 6-7 GPa although values are uncertain because of the lack of a clear-cut method of evaluation stress levels from these particular wave profiles.

Chaotic motion of the measured velocity history initiates very shortly after wave arrival. The two profiles compare only in the rough nature of the wave, in the approximate final amplitudes, and in the approximate arrival and shape of the release waves (see Figure 3). Irregular motions in the velocity history suggest a deformation process which is coarse in its spatial features and brittle in the sense that acoustic emissions occur in the faulting process and contribute to the irregular motions observed at the recording interface.

To summarize results of the lower amplitude wave profile experiments, unusual features are observed which hint at a complex time-dependent failure process. The tests conducted to about 4.5 GPa are largely elastic in there wave profile characteristics but even here there are indications of some inelastic processes. The tests to 6-7 GPa show clear indications of dynamic failure. There is no evidence for an unambiguous Hugoniot elastic limit.

Wave Velocity Features

In Figure 5 the velocities of significant features in the measured wave profiles are displayed. It is emphasized that the velocities shown for compressed states are Lagrangian wave speeds. Other velocity features are plotted against their corresponding current or Hugoniot state particle velocity.

Velocities of the compression wave are displayed through the continuous velocity of the precursor envelope and the discrete shock velocities of the four higher impact amplitude experiments. The three higher shock velocity points are nicely fit to a linear shock-velocity-versus-particle-velocity relation, $U = C_o + Su$, with C_o = 2.01 km/s and S = 1.7. The lowest shock velocity data point falls slightly below this fit but the large risetime of this wave made it difficult to determine the wave speed with comparable certainty.

The linear behavior in the region of the higher compression data provides an analytic relation for the compression,

$$\Delta\sigma = \frac{\rho_o C_o^2 \Delta\varepsilon}{(1 - S\Delta\varepsilon)^2}, \qquad (1)$$

where $\Delta\sigma$ and $\Delta\varepsilon$ are jumps in stress and strain through the shock and $\varepsilon = 1 - \rho_o / \rho$. Consequently, a wave speed associated with the slope of the Hugoniot can be defined through, $\rho_o c_H = \rho\sqrt{d\sigma / d\rho}$. In Figure 5 c_H is shown within the range of the shock velocity data from which it was derived.

A measure of the sonic velocity at the compressed state determined from first arrival of the release wave has been determined from the eight tests (Figure 5). Sonic velocities for the four highest amplitude tests lie well above the c_H curve suggesting elastic rigidity in the initial decompression response. Assuming constant Poisson's ratio the bulk velocities, $c_o = \sqrt{(1+\nu)/3(1-\nu)}c_L$, fall slightly above the c_H curve. This argument supports little irreversible densification of the glass on the Hugoniot over the 10-25 GPa Hugoniot stress range. On the other hand if measured sonic velocities characterize bulk release, substantial densification is indicated.

Second Shock Data

Second shock (or reshock) velocities were determined from the measurements. These velocities lie above the corresponding first shock

velocities but below the curve identifying the slope of the Hugoniot. Based on the relation $\gamma_{eff} = \upsilon \Delta p / \Delta E|_{\upsilon}$, an effective Gruneisen was estimated from the data.

The values for γ_{eff} of x, x, x, and x were, respectively, estimated for the increasing second shock states. The experimental values may reflect indicate additional densification (4-fold to 6-fold SiO_2 crystal structure) brought about by the double shock process. Alternatively the principal Hugoniot and secondary shock states may reflect material strength characteristics persisting at the experimental stress levels (10-25 GPa).

Conclusions

Compression wave profiles on soda-lime glass do not provide evidence of a distinct Hugoniot elastic limit. Profile data to a peak compression of 4.6 GPa shows evidence for time-dependent inelastic deformation – possibly densification in the SiO_2 glass structure. Profile data to peak compression of 6-7 GPa indicate transition to a coarse catastrophic failure process – possibly brittle shear fracture on a relatively large spatial scale. Principal and second shock data to nearly 30 GPa show some evidence for transition to the expected higher density SiO_2 phase, but densities achieved within this range are not yet consistent with the high pressure phase. Gruneisen parameter properties are estimated from first and second shock data and show some anomalies.

Acknowledgments

The authors would like to acknowledge support for the present research from Alliant Tech Systems under the direction of Tim Holmquist and from the Joint DoD/DOE MOU on munitions technology.

References

Brar, N. S., S. J. Bless and Z. Rosenberg, Impact-Induced Failure Waves in Glass Bars and Plates, Appl. Phys. Lett. 59, 3396-398 (1991).

Bourne, N. K., and Z. Rosenberg, The Dynamic Response of Soda-Lime Glass, in Shock Compression of Condensed Matter - 1991, S. C. Schmidt and W. C. Tao, eds., Elsevier, pp. 567-572 (1996).

Dandekar, D. P. and P. A. Beaulieu, Failure Waves under Shock Wave Compression in Soda Lime Glass, in Metallurgical and Materials Applications of Shock Waves and High Strain Rate Phenomena, L. E. Murr, K. P. Staudhammer and M. A. Meyers, eds., Elsevier, pp. 211-218 (1995).

Anderson, C. E., V. Hohler, J. D. Walker and A. J. Stilp, Penetration of Long Rods into Steel and Glass Target: Experiment and Computation, in Proc. 14th Int. Symp. on Ballistics, Quebec City, Canada, pp. 145-154 (1993).

Holmquist, T.J., G. R. Johnson, D. E. Grady, C. M. Lopatin and E. J. Hertel, High Strain Rate Properties and Constitutive Modeling of Glass, in Proc. 14th Int. Symp. on Ballistics, Jerusalem, Israel, pp. 237-244 (1995).

Kanel, G. I., S. V. Rasorenov and V. E. Fortov, Failure Waves and Spallation in Homogeneous Brittle Materials, in Shock Compression of Condensed Matter - 1991, S. C. Schmidt, R. C. Dick, J. W. Forbes and D. G. Tasker eds., Elsevier, pp. 451-454 (1992).

Rasorenov, S. V., G. I. Kanel, V. E. Fortov and M. M. Abasehov, The Fracture of Glass under High-Pressure Impulsive Loading, in High Pressure Research, Vol. 6, Gordon and Breech, pp. 225-232 (1991).

Rosenberg, Z., D. Yaziv and S. J. Bless, Spall Strength of Shock Loaded Glass, J. Appl. Phys., 58, 3249 (1985).

Senf, H., E. Strassburger and H. Rothenhausler, Stress Wave Induced Damage and Fracture in Impacted Glasses, in EuroDymat 94 - International Conference on Mechanical and Physical Behavior of Materials Under Dynamic Loading, les editions de physics, pp. 741 (1994).